Electrochimica Acta 88 (2013) 66–73

Contents lists available at SciVerse ScienceDirect

Electrochimica Acta

journal homepage: www.elsevier.com/locate/electacta

# Catalytic EC′ reaction at a thin film modified electrode

Leandro Gerbino, Ana M. Baruzzi, Rodrigo A. Iglesias*

*Departamento de Fisicoquímica, Facultad de Ciencias Químicas, Universidad Nacional de Córdoba, INFIQC, CONICET, Pabellón Argentina Ala 1 Piso 2, Ciudad Universitaria, Córdoba 5000, Argentina*

ARTICLE INFO

*Article history:*
Received 12 June 2012
Received in revised form 11 October 2012
Accepted 12 October 2012
Available online 22 October 2012

*Keywords:*
Numerical simulation
EC′ reaction
Thin film
Finite difference
Catalytic reaction

ABSTRACT

Numerical simulations of cyclic voltammograms corresponding to a catalytic EC′ reaction taking place at a thin film modified electrode are performed by way of finite difference method. Besides considering the chemical kinetic occurring inside the thin film, the model takes into account the different diffusion coefficients for each species at each of the involved phases, i.e. the thin film layer and bulk solution. The theoretical formulation is given in terms of dimensionless model parameters but a brief discussion of each of these parameters and their relationship to experimental variables is presented.

Special emphasis is given to the use of working curve characteristics to quantify diffusion coefficient, homogeneous kinetic constant and thickness of the thin layer in a real system.

Validation of the model is made by comparison of experimental results corresponding to the electron charge transfer of $Ru(NH_3)_6^{3+}/Ru(NH_3)_6^{2+}$ hemi-couple at a thin film of a cross-linked chitosan film containing an immobilized redox dye.



## 1. Introduction

The efficiency in the immobilization of sensing molecules is one of the most important steps to achieve a good performance in many analytical devices [1]. Electrochemical biosensors for instance, involve the immobilization of biomolecules namely enzymes [2,3], nucleic acids [4], antigens or antibodies [5], resulting in devices of high specificity. Optical sensors, on the other hand, involve the immobilization of dyes inside different type of substrates using mechanical entrapment [6,7], electrostatic interactions [8–10] or covalent immobilization [11–13].

Polymers used with this purpose, especially those ion-conducting or polyelectrolytes, have become important due to their mechanical properties, high diffusion rate of ions and in many cases biocompatibility [14]. Advantages and disadvantages of physical and chemical interactions between matrix and dye have been reported; physical interaction results in a loss of the entrapped molecule, while covalent immobilization is by far the best approach to stabilize the molecules inside the matrix; but on the other hand, the activity of crosslinked biomolecules in the case of biosensors or the optical properties of immobilized dyes in the case of optodes, and consequently the response of the sensors may be affected by a strong interaction with the matrix [15,3].

To study the electrochemical response of these systems, a theoretical background that correlates with experimental approaches is needed and is also a useful tool to be able to predict their behavior.

We have previously reported the immobilization of thionine in crosslinked chitosan films and evaluated the acid–base and redox properties of this dye immobilized in the polymeric matrix [15]. We demonstrated that thionine was effectively immobilized inside the crosslinked chitosan matrix and that this composite shows excellent filmogenic properties. To analyze its redox properties, the electron transfer of a Ru amine complex at the dye containing film modified electrode was analyzed. It was shown that thionine retains its redox activity and that not only diffusion control but also the kinetics of the coupled chemical reaction determine the rate of the dye reduction.

In the present paper we report numerical simulations of cyclic voltammetry (CV) experiments, corresponding to a general and global process that considers diffusion in solution and across a thin polymer film coupled to a catalytic EC′ reaction occurring inside the thin film. This model was solved by finite difference method using two-points discretization for all derivatives [16,17]. Under given conditions the numerical model can predict the proposed mechanism for the mentioned experimental system.

## 2. Experimental

### 2.1. Materials

Chitosan of low molecular weight from the shrimp shell with a degree of deacetylation of 83.3% and thionine acetate were

* Corresponding author. Tel.: +54 351 4334169/80x107/110; fax: +54 351 4334188.
*E-mail address:* riglesias@mail.fcq.unc.edu.ar (R.A. Iglesias).

0013-4686/$ – see front matter © 2012 Elsevier Ltd. All rights reserved.
http://dx.doi.org/10.1016/j.electacta.2012.10.043

purchased from Sigma–Aldrich. Acetic acid and glutaraldehyde 25% were obtained from J.T. Baker. Hexaammineruthenium (III) chloride, $Ru(NH_3)_6Cl_3$, 99%, was purchased from Strem Chemicals. All chemicals were of analytical grade and used without further purification; and the solutions were prepared with ultrapure water (Milli Q–Milli RO system).

### 2.2. Instrumentation, cell and electrodes

Electrochemical measurements were performed using an AUTOLAB PGSTAT101 potentiostat/galvanostat. Experiments were made in a standard three electrodes glass cell. A polycrystalline gold disk was used as working electrode for the experiments done with different film thickness in the absence of thionine and for the comparative experiments in presence and absence of thionine; the area was 0.042 $cm^2$. A platinum foil was used as counter-electrode and the interface defined by (Ag|AgCl|KCl, 3M) was used as a reference electrode. All experimental potentials are referred to this interface.

### 2.3. Preparation of crosslinked chitosan film on gold electrode

Crosslinked chitosan films on gold (CHI|Au) were prepared using glutaraldehyde as the crosslinking agent according to the following procedure. Chitosan of low molecular weight was used to prepare a 2% (w/v) solution using acetic acid solution (2%, v/v). After dissolution of the chitosan powder the solution was filtered and preserved in a colored flask. A volume of 2.50 mL of this solution was mixed with 320 μL of glutaraldehyde solution (5%, v/v in water) and acetic acid solution (2%, v/v) was added to obtain different total volume amounts of reaction mixture (6 mL, 120 mL, 200 mL and 250 mL). The modified electrodes obtained with these reactions mixtures are denominated as CHI|Au6, CHI|Au120, CHI|Au200 and CHI|Au250 respectively. Immediately, each final mixture was drop-casted onto a polycrystalline gold electrode and left to react during 24 h at room temperature, in an almost water saturated chamber. In this way, several film thicknesses were obtained, depending on the chitosan concentration of each solution mixture.

### 2.4. Preparation of crosslinked chitosan film containing thionine dye

Dye-containing films were prepared using the CHI|Au6 reaction mixture with the addition of 100 μL of 0.01 M thionine solution. This final mixture (THI|CHI) was cast on the disc gold electrode and left during 48 h until solvent evaporation.

## 3. Theory

### 3.1. Model description

Fig. 1 depicts the model system and reaction mechanism to be simulated, which implies that species O can be reduced at a thin film modified electrode and regenerated by a coupled homogeneous chemical reaction occurring with the electrochemical product R and a redox immobilized species (Q). Diffusion is allowed only for O and R at lower rates inside the thin film than in solution. Q and its chemical product (T) are restricted to exist inside the thin film where their diffusion is forbidden.

Several differential equations have to be solved for each species depending on their location. Fick's second law and a term given by the catalytic homogenous reaction define the differential equation for each species inside the thin film ($0 < x \leq d$) as follows:

$$\frac{\partial C_O(x,t)}{\partial t} = D_O^{TF}\frac{\partial^2 C_O(x,t)}{\partial x^2} + k_c C_R(x,t) C_Q(x,t) \quad (1)$$

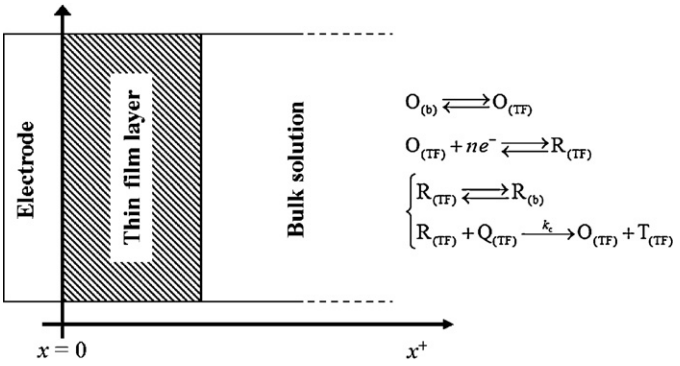


**Fig. 1.** Scheme and reaction mechanism for the simulation model of a catalytic EC′ reaction taking place at a thin film modified electrode. Positive distance is taken from the electrode surface to the bulk solution. Subscript (b) and (TF) indicate species in solution or inside the thin film respectively.

$$\frac{\partial C_R(x,t)}{\partial t} = D_R^{TF}\frac{\partial^2 C_R(x,t)}{\partial x^2} - k_c C_R(x,t) C_Q(x,t) \quad (2)$$

$$\frac{\partial C_Q(x,t)}{\partial t} = -k_c C_R(x,t) C_Q(x,t) \quad (3)$$

$$\frac{\partial C_T(x,t)}{\partial t} = k_c C_R(x,t) C_Q(x,t) \quad (4)$$

being $x$ the distance from the electrode surface, $t$ the experimental time, $D_O^{TF}$ and $D_R^{TF}$ the diffusion coefficient for O and R inside the thin film respectively, $k_c$ the homogeneous kinetic constant and $C_i$ ($i$ = O, R, Q or T) the concentration of each species.

As the catalytic chemical reaction is restricted to occur inside the thin film, simple Fick's second law should be solved for O and R in the solution ($x > d$) given by:

$$\frac{\partial C_O(x,t)}{\partial t} = D_O^{b}\frac{\partial^2 C_O(x,t)}{\partial x^2} \quad (5)$$

$$\frac{\partial C_R(x,t)}{\partial t} = D_R^{b}\frac{\partial^2 C_R(x,t)}{\partial x^2} \quad (6)$$

where $D_O^b$ and $D_R^b$ are the diffusion coefficients of O and R in solution respectively.

There are not differential equations for Q and T to be solved in this latter phase.

Initial conditions for the concentration of each species in the full length of the system are defined as follows:

$$t = 0: \begin{cases} C_O(x,t) = C_O^0 \\ C_R(x,t) = C_O^0 \exp\left[\dfrac{nF}{RT}(E - E^{0'})\right] \end{cases} \quad \forall x \geq 0 \quad (7)$$

$$t = 0: \begin{cases} C_Q(x,t) = C_Q^0 \\ C_T(x,t) = 0 \end{cases} \quad \forall 0 < x \leq d \quad (8)$$

$$t = 0: \begin{cases} C_Q(x,t) = 0 \\ C_T(x,t) = 0 \end{cases} \quad \forall x > d \quad (9)$$

being $C_O^0$ the initial (bulk) concentration of O, $C_Q^0$ the initial concentration of Q inside the thin film, $d$ the thin film thickness and $E^{0'}$ the formal reduction potential; $n$, $F$, $R$, $T$ and $E$ are the electron number involved in the redox reaction, the Faraday constant, the ideal gas constant, the temperature and the applied potential respectively.

Boundary conditions should be defined at the electrochemical interface ($x = 0$), at the outer boundary of the thin film ($x = d$) and at the outer boundary of the solution ($x \to \infty$).

- At the interface the flux continuity between O and R must be fulfilled at any time and it is given by:

$$D_O^{TF}\left.\frac{\partial C_O(x,t)}{\partial x}\right|_{x=0} = -D_R^{TF}\left.\frac{\partial C_R(x,t)}{\partial x}\right|_{x=0} \quad (10)$$

subject to a reversible electron transfer which defines the relationship between the interfacial concentration of O and R through a Nernst equation as follows:

$$\frac{C_O(0,t)}{C_R(0,t)} = \exp\left[\frac{nF}{RT}(E - E^{0'})\right] \quad (11)$$

- At the outer film boundary, diffusing species can cross this plane and their flux continuity, both sides of this limit, ensures mass conservation:

$$\lim_{x<d,\ x\to d} D_i^{TF}\frac{\partial C_i(x,t)}{\partial x} = \lim_{x>d,\ x\to d} D_i^{b}\frac{\partial C_i(x,t)}{\partial x} \quad \text{with } i = \text{O or R} \quad (12)$$

On the other side, immobilized species (Q and T) without any flux coming from the bulk solution define a zero flux boundary condition that can be written as follows:

$$D_Q^{TF}\left.\frac{\partial C_Q(x,t)}{\partial x}\right|_{x=d} = 0 \quad \text{and} \quad D_T^{TF}\left.\frac{\partial C_T(x,t)}{\partial x}\right|_{x=d} = 0 \quad (13)$$

- At the outer solution boundary, semi-infinite linear diffusion regime, the system is not perturbed by the electrochemical reaction and the concentration of O and R remains equal as at the beginning of the simulation; this can be written as:

$$x \to \infty : \begin{cases} C_O(x,t) = C_O^0 \\ C_R(x,t) = 0 \end{cases} \quad \forall t \geq 0 \quad (14)$$

### 3.2. Discretization and formulation of dimensionless parameters for CV experiments

A reference time $\tau = RT(nF\nu)^{-1}$ can be divided into $N_P$ intervals in order to obtain the time interval for the simulation ($\delta t$) and a dimensionless time scale as follows:

$$\delta t = \frac{\tau}{N_P}$$

$$t_N = \frac{j}{N_P}$$

where $j$ is the index for time discretization and $t_N$ the dimensionless time.

The applied potential during cyclic voltammetry can be mathematically written as:

$$E = \begin{cases} E_o - \nu t & \forall t < \lambda \\ E_o - 2\nu\lambda + \nu t & \forall t \geq \lambda \end{cases} \quad (15)$$

and considering the time discretization, a dimensionless potential ($P_j$) can be defined as follows:

$$P_j = \begin{cases} P_o - \dfrac{j}{N_P} & \forall j < \lambda_N N_P \\ P_o - 2\lambda_N + \dfrac{j}{N_P} & \forall j \geq \lambda_N N_P \end{cases} \quad (16)$$

being $P_o = nFE_o(RT)^{-1}$ the starting dimensionless potential and $\lambda_N = \lambda\tau^{-1}$ the switching dimensionless time of the cyclic potential scan.

In a similar way, distance away from the electrode, defined as the positive direction, can be discretized as:

$$\begin{cases} x = ih^{TF} & \forall x \leq d \text{ or } i \leq N_c^{TF} \\ x = N_c^{TF}h^{TF} + (i - N_c^{TF})h^b & \forall x > d \text{ or } i > N_c^{TF} \end{cases} \quad (17)$$

being $h^{TF}$ and $h^b$ the distance intervals for the simulation inside the thin film layer or adjacent solution respectively, $i$ the distance index and $N_c^{TF}$ the number of intervals in which the thin film layer is divided.

A potential value applied at the interface changes the interfacial concentrations of O and R according to the Nernst equation (Eq. (11)) and these latter concentrations can be calculated using a discretized form of Eq. (10):

$$D_O^{TF}\frac{C_O(h^{TF},t) - C_O(0,t)}{(h^{TF}/2)} \cong -D_R^{TF}\frac{C_R(h^{TF},t) - C_R(0,t)}{(h^{TF}/2)} \quad (18)$$

This discretization considers the metal–solution interface as a plane located just the left boundary of the first distance interval. In this way, the approximation has an error of $O[(h^{TF})^2]$, the same error order of the discretized formulae used to compute diffusion (see below).

Replacement of Eq. (11) on Eq. (18) and after some rearrangement the following expressions, which allows for the computation of the interfacial concentrations of R and O, are obtained:

$$f_R(0,j) = \frac{C_R(0,j)}{C_O^0} = \frac{f_R(1,j) + \zeta_1 f_O(1,j)}{1 + \zeta_1 \exp(P_j)} \quad (19)$$

$$f_O(0,j) = \frac{C_O(0,j)}{C_O^0} = f_R(0,j)\exp(P_j) \quad (20)$$

being $\zeta_1 = D_O^{TF}(D_R^{TF})^{-1}$.

Concentration values at any point inside the thin film layer ($0 < x < d$ or $0 < i < N_c^{TF}$) can be computed by discretization of Eq. (1) to Eq. (4), considering a two-point and three point derivatives for time and distance respectively [16]:

If $i = 1$:

$$\begin{aligned} f_O(1,j+1) &= f_O(1,j) + D_{O,M}^{TF}[f_O(2,j) - 3f_O(1,j) + 2f_O(0,j)] \\ f_R(1,j+1) &= f_R(1,j) + D_{R,M}^{TF}[f_R(2,j) - 3f_R(1,j) + 2f_R(0,j)] \end{aligned} \quad (21)$$

If $i > 1$:

$$\begin{aligned} f_O(i,j+1) &= f_O(i,j) + D_{O,M}^{TF}[f_O(i+1,j) - 2f_O(i,j) + f_O(i-1,j)] + k_{c,M}f_R(i,j)f_Q(i,j) \\ f_R(i,j+1) &= f_R(i,j) + D_{R,M}^{TF}[f_R(i+1,j) - 2f_R(i,j) + f_R(i-1,j)] - k_{c,M}f_R(i,j)f_Q(i,j) \end{aligned} \quad (22)$$

If $i \geq 1$:

$$f_Q(i,j+1) = f_Q(i,j) - k_{c,M}f_R(i,j)f_Q(i,j) \quad (23)$$

$$f_T(i,j+1) = f_T(i,j) + k_{c,M}f_R(i,j)f_Q(i,j) \quad (24)$$

where $D_{O,M}^{TF} = D_O^{TF}\delta t\,(h^{TF})^{-2}$ and $D_{R,M}^{TF} = D_R^{TF}\delta t\,(h^{TF})^{-2}$ are the model diffusion coefficients of O and R respectively while $k_{c,M} = k_c C_O^0 \delta t$ is the dimensionless chemical kinetic constant.

Details of discretized expressions presented in Eqs. (21)–(24) can be found elsewhere [16,17].

Just at the outer film boundary ($x = d$), the species concentrations can be computed by discretization of boundary conditions given by Eqs. (12) and (13), which after some rearrangement give Eqs. (25)–(28) respectively:

$$f_O(N_c^{TF}, j) = \frac{f_O(N_c^{TF}+1, j) + \zeta_2\theta f_O(N_c^{TF}-1, j)}{1+\zeta_2\theta} \quad (25)$$

$$f_R(N_c^{TF}, j) = \frac{f_R(N_c^{TF}+1, j) + \zeta_3\theta f_R(N_c^{TF}-1, j)}{1+\zeta_3\theta} \quad (26)$$

$$f_Q(N_c^{TF}, j) = f_Q(N_c^{TF}-1, j) \quad (27)$$

$$f_T(N_c^{TF}, j) = f_T(N_c^{TF}-1, j) \quad (28)$$

where $\zeta_2 = D_O^{TF}(D_O^b)^{-1}$, $\zeta_3 = D_R^{TF}(D_R^b)^{-1}$ and $\theta = h_b(h_{TF})^{-1}$.

Beyond the outer film boundary ($x > d$), only O and R can exist and their concentrations can be computed with discretized forms of Eqs. (5) and (6):

$$f_O(i, j+1) = f_O(i,j) + D_{O,M}^b[f_O(i+1,j) - 2f_O(i,j) + f_O(i-1,j)] \quad (29)$$

$$f_R(i, j+1) = f_R(i,j) + D_{R,M}^b[f_R(i+1,j) - 2f_R(i,j) + f_R(i-1,j)] \quad (30)$$

Using the previous equations, from Eqs. (19)–(30), iterative solution for any species concentrations at every distance and time can be computed.

In order to better analyze the obtained results, other dimensionless parameters need to be defined.

Considering the relationship between the model diffusion coefficients with the distance interval inside the thin film ($D_{O,M}^{TF} = D_O^{TF}\delta t(h^{TF})^{-2}$ or $D_{R,M}^{TF} = D_R^{TF}\delta t(h^{TF})^{-2}$) and the stability criterion for an explicit finite difference method ($D_{O,M}^{TF} \le 0.5$ and $D_{R,M}^{TF} \le 0.5$), a dimensionless interval distance ($h_N^{TF}$) can be defined, inside the thin film layer, by:

$$h_N^{TF} = \frac{1}{\sqrt{0.45N_P}} = \frac{h^{TF}}{\sqrt{D_{max}^{TF}\tau}} \quad \text{being} \quad D_{max}^{TF} = \max(D_O^{TF}, D_R^{TF}) \quad (31)$$

which in turn allows for the computation of a dimensionless distance scale as:

$$x_N = ih_N^{TF} \quad \forall i \le N_c^{TF} \quad (32)$$

It should be noted that we have used a maximum model diffusion coefficient of 0.45 (see Eq. (31)) instead of the 0.5 value given by the stability criterion. We have tested both values in our simulations and we obtained identical results. However, we preferred to use a lower value because Feldberg [18] has reported instabilities during potential step simulations when the limiting value of 0.5 is used, which are minimized when a 0.45 value is implemented. Also, Bieniasz [19] has published a detailed analysis of the lack of stability when a model diffusion coefficient of 0.5 is used for mechanisms involving coupled homogeneous reactions.

These latter definitions allows for the dimensionless film thickness ($\vartheta$) to be expressed as:

$$\vartheta = \frac{d}{\sqrt{D_{max}^{TF}\tau}} = N_c^{TF}h_N^{TF} \quad (33)$$

In a similar way, beyond the outer film boundary, dimensionless distance can be defined in terms of the following equation:

$$x_N = N_c^{TF}h_N^{TF} - (i - N_c^{TF})h_N^b \quad \forall i > N_c^{TF} \quad (34)$$

being:

$$h_N^b = \frac{1}{\sqrt{0.45N_P}} = \frac{h^b}{\sqrt{D_{max}^b\tau}} \quad \text{being} \quad D_{max}^b = \max(D_O^b, D_R^b)$$

The faradaic current is related to the interfacial concentration profile as:

$$I(t) = -nFA\left(\frac{\partial C_O}{\partial x}\right)\Big|_{x=0} \quad (35)$$

and it can be computed as:

$$I_j = -nFAD_O^{TF}C_O^0\frac{f_O(1,j) - f_O(0,j)}{h_{TF}} \quad (36)$$

If dimensionless parameters are introduced in the previous expression a dimensionless current ($\chi_j$) is obtained:

$$\chi_j = \frac{I_j\sqrt{D_{max}\tau}}{nFAD_O^{TF}C_O^0} = -\frac{f_O(1,j) - f_O(0,j)}{h_N^{TF}} \quad (37)$$

## 4. Results and discussion

According to the theoretical development (see Section 3), all results are presented in terms of dimensionless parameters, i.e. the experimental variables of the system are related to the model parameters as:

Dimensionless film thickness:

$$\vartheta = \frac{d}{\sqrt{D_{max}^{TF}\tau}}$$

Dimensionless diffusion constants:

$$\zeta_1 = D_O^{TF}(D_R^{TF})^{-1}$$

$$\zeta_2 = D_O^{TF}(D_O^b)^{-1}$$

$$\zeta_3 = D_R^{TF}(D_R^b)^{-1}$$

Dimensionless kinetic constant:

$$k_{c,M} = k_c C_O^0 \delta t$$

Normalized redox species concentration inside film:

$$f_S(i,j) = \frac{C_S(i,j)}{C_O^0}$$

One of the main advantages of finite difference methods applied to electrochemical systems is their capability to simulate the diffusion using different diffusion coefficients for each species involved. Specifically, Eqs. (21), (22), (29) and (30) show that different diffusion coefficients can be used for each species in each phase.

As a matter of simplicity, we decided to use the same diffusion coefficient for every species in the same phase. The results of the simulation show that it is more important the difference of the coefficients at different phases. All simulations were repeated with increasing number of simulation steps until a convergence of at least 1% was reached.

### 4.1. Heterogeneous charge transfer

Fig. 2 shows two sets of cyclic voltammograms corresponding to the heterogeneous electron transfer of the species O initially in solution at a thin film modified electrode with different dimensionless thickness ($\vartheta$). Voltammograms in Fig. 2(a) were obtained with diffusion coefficient values for the soluble species inside the thin layer that are two orders of magnitude higher than those shown in Fig. 2(b). Almost the same general behavior can be observed in both figures, lower is the thickness and higher is the dimensionless reduction peak current of the voltammetric profile. Moreover, when the diffusion across the thin layer decreases, a tendency to reach a limiting current can be seen when voltammograms with

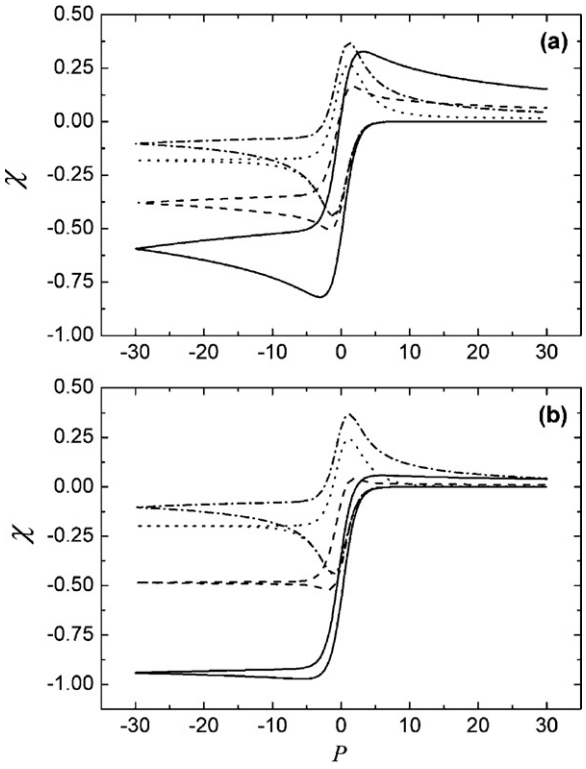


**Fig. 2.** Dimensionless cyclic voltammograms for a reversible electron transfer at a thin film modified electrode with different dimensionless thickness. (––––) $\vartheta = 1.0$, (– – –) $\vartheta = 2.0$, (·····) $\vartheta = 5.0$, (–·–·–·–) $\vartheta = 30$. (a) $-\log\zeta_2 = -\log\zeta_3 = 2.0$ and (b) $-\log\zeta_2 = -\log\zeta_3 = 4.0$. Other simulation parameters: $P_o = 30.0$, $P_f = 30.0$, $\zeta_1 = 1.0$, $f_O^0 = 1.0$, $N_P = 750$.

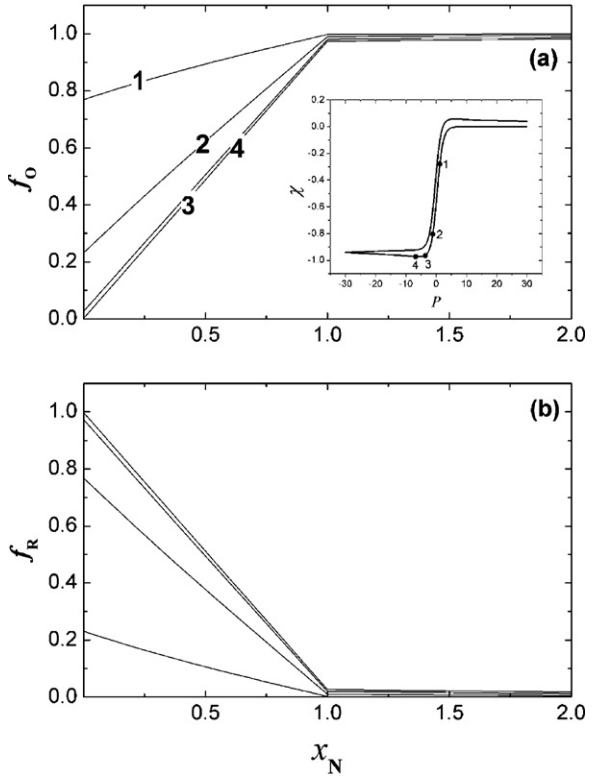


**Fig. 3.** Dimensionless concentration profiles obtained during the evolution of a cyclic voltammogram. $\vartheta = 1.0$, $-\log\zeta_2 = -\log\zeta_3 = 4.0$. (a) $f_O(x_N)$ and (b) $f_R(x_N)$. Other simulation parameters as in Fig. 2. Inset: corresponding cyclic voltammogram. Concentration profiles correspond to the points defined in the inset.

the same $\vartheta$ parameter are compared. For instance, when $\vartheta = 1$, a limiting current can be observed during the reduction scan in Fig. 2(b), while a peak shaped voltammogram is still evident in Fig. 2(a). On the other hand, high values of $\vartheta$ give the same voltammetric profile with the common characteristics of a reversible and diffusion controlled electron transfer. To better understand the voltammetric behavior, Fig. 3 shows the dimensionless concentration profiles of O and R at different points during the potential sweep. As it can be seen, for instance in Fig. 3(a), the concentration profile of O inside the film is nearly linear with a constant diffusion layer defined by the dimensionless thickness ($\vartheta = 1.0$ in this particular case). As the interfacial concentration of O decreases, the interfacial concentration gradient becomes higher and so the corresponding dimensionless current. When the interfacial concentration of O is close to zero, at around −5 units of dimensionless potential ($P_j$), a limiting current is observed. In this case, and wherever a limiting current is observed, the solution acts as a sink of O that keeps almost constant the concentration of this species at the outer boundary of the film, where O has a much lower diffusion rate.

It is evident that the shape and size of the voltammetric profiles are markedly dependent on the relative diffusion rate inside the thin film and the size of the dimensionless thickness. Considering this, the best approach to quantify experimental variables is by fitting of the full voltammetric shape; however the dependence of the dimensionless reduction current with the dimensionless thickness is univocally defined by the dimensionless diffusion constant $\zeta_2$ and characteristic working curves can be built in order to quantify these latter variables. Four of these curves are shown in Fig. 4 for the reduction (Fig. 4(a)) and oxidation (Fig. 4(b)) dimensionless current peaks. Several aspects should be noted:

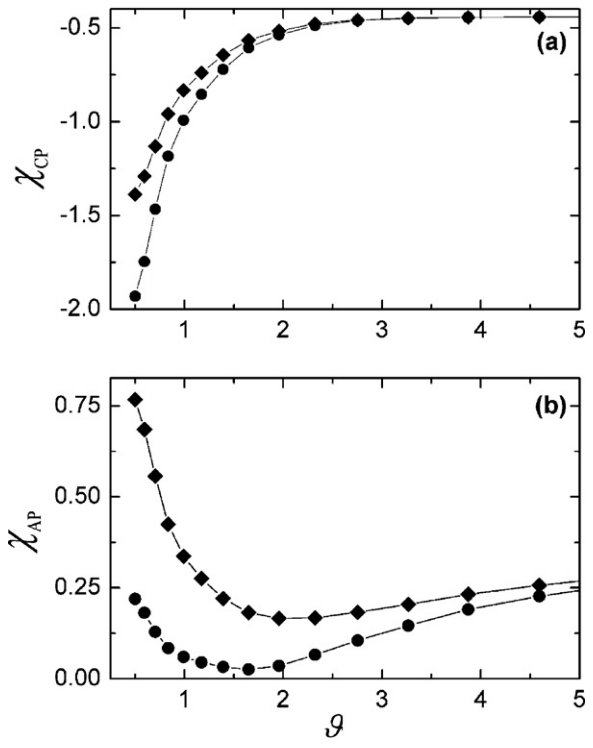


**Fig. 4.** Dimensionless current peak values as a function of the dimensionless thickness of the film. (♦) $-\log\zeta_2 = -\log\zeta_3 = 2.0$. (●) $-\log\zeta_2 = -\log\zeta_3 = 4.0$. (a) reduction peak current, $\chi_{CP}$ and (b) oxidation peak current, $\chi_{AP}$. Other parameters as in Fig. 2.

**Table 1**
Polynomial fitting parameters corresponding to the relationship between dimensionless reduction peak current ($\chi$) and dimensionless thickness ($\vartheta$) for different dimensionless diffusion constant ($\zeta_2$). The corresponding polynomial function is given by $\chi(\vartheta) = a_0 + a_1\vartheta + a_2\vartheta^2 + \cdots + a_8\vartheta^8$.

| Polynomial parameters | $-\log\zeta_2$ | | | |
|---|---|---|---|---|
| | 1 (0.9992)[a] | 2 (0.9989)[a] | 3 (0.9991)[a] | 5 (0.9991)[a] |
| $a_0$ | −1.318 | −2.862 | −5.58 | −7.14 |
| $a_1$ | 1.158 | 4.29 | 14.2 | 19.5 |
| $a_2$ | −0.648 | −3.48 | −19.7 | −27.8 |
| $a_3$ | 0.187 | 1.58 | 16.2 | 23.1 |
| $a_4$ | −0.0274 | −0.405 | −8.2 | −11.8 |
| $a_5$ | 0.0016 | 0.054 | 2.57 | 3.7 |
| $a_6$ | – | −0.0029 | −0.48 | −0.69 |
| $a_7$ | – | – | 0.050 | 0.072 |
| $a_8$ | – | – | −0.0022 | −0.0031 |

[a] $R$-square value for the polynomial fitting in parenthesis.

- At sufficiently high dimensionless thickness, working curves reach a constant value. This happens when the diffusion length is lower than the film thickness.
- Working curves are useful if dimensionless thickness smaller than two units ($\vartheta < 2$) can experimentally be accessed. This can be done by decreasing the thin film thickness or the sweep potential rate (see the end of this section).
- Reduction current peaks are more useful than oxidation peaks to build these working curves because oxidation peak currents are smaller, close to zero in some cases and difficult to measure.

In order to use the latter working curves, without performing the numerical simulations given, Table 1 summarizes the fitting parameters ($a_k$, $k = 0, \ldots, 8$), obtained with an 8th order polynomial, for several working curves corresponding to different values of the dimensionless diffusion constant $\zeta_2$.

It was claimed before that dependences of reduction current with the dimensionless film thickness are different for a range of $\vartheta < 2$. This condition can be experimentally fulfilled at small enough values of actual film thickness or enough low sweep potential rates, both cases allow for the diffusion layer to evolve beyond the actual film thickness. Considering a typical diffusion coefficient ($D^{TF}_{max} \approx 10^{-6}\text{cm}^2\text{s}^{-1}$) the maximum value for the actual film thickness, in order to observe the previous characteristics, is given by:

$$\vartheta = \frac{d}{\sqrt{D^{TF}_{max}\tau}} < 2 \Rightarrow d\sqrt{\nu} < 2\sqrt{\frac{D^{TF}_{max}RT}{nF}}$$

Therefore, if the sweep potential rate has a value close to $0.10\,\text{V s}^{-1}$ the actual film thickness should be smaller than $\approx 10\,\mu\text{m}$.

### 4.2. Catalytic homogeneous reaction

The incorporation of a catalytic homogeneous reaction inside the thin film that can regenerate the electroactive starting material has the effect of "buffering" the decrease of electroactive species inside the thin film. Fig. 5 shows the dimensionless voltammograms obtained for different thicknesses of the thin film when the kinetics of the coupled chemical reaction is noticeable. The same figure shows the corresponding profile in absence of coupled chemical reaction. It can be noted that the reduction current for the three considered situations are similar when the coupled chemical reaction takes place; however the corresponding voltammetric profiles with no chemical reaction occurring are markedly different for the calculated thicknesses. Of course, the reduction current, markedly depend on the kinetic constant and concentrations of the involved species as can be noted from the plots depicted in Fig. 6.

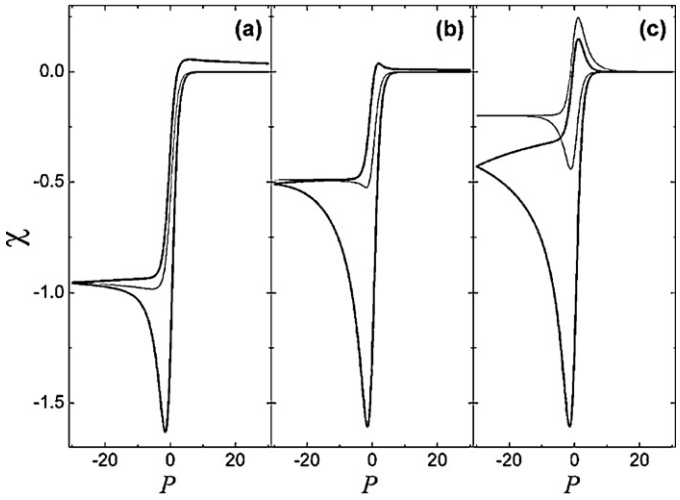


**Fig. 5.** Dimensionless cyclic voltammograms for a reversible electron transfer with ((——) $k_{c,M} = 1.0 \times 10^{-3}$, $f^0_Q = 10.0$) and without ((—) $k_{c,M} = 0.0$, $f^0_Q = 0.0$) a following irreversible redox reaction taking place at a thin film modified electrode. (a) $\vartheta = 1.0$, (b) $\vartheta = 2.0$ and (c) $\vartheta = 5.0$. Other simulation parameters: $P_o = 30.0$, $P_f = -30.0$, $\zeta_1 = 1.0$, $-\log\zeta_2 = -\log\zeta_3 = 2.0$, $N_P = 1000$.

One aspect that should be noted is the difference between results shown in Fig. 6 with those described previously in Fig. 4. It can be concluded that diffusional effects (i.e. diffusional control over the faradaic current) are more noticeable at small dimensionless film

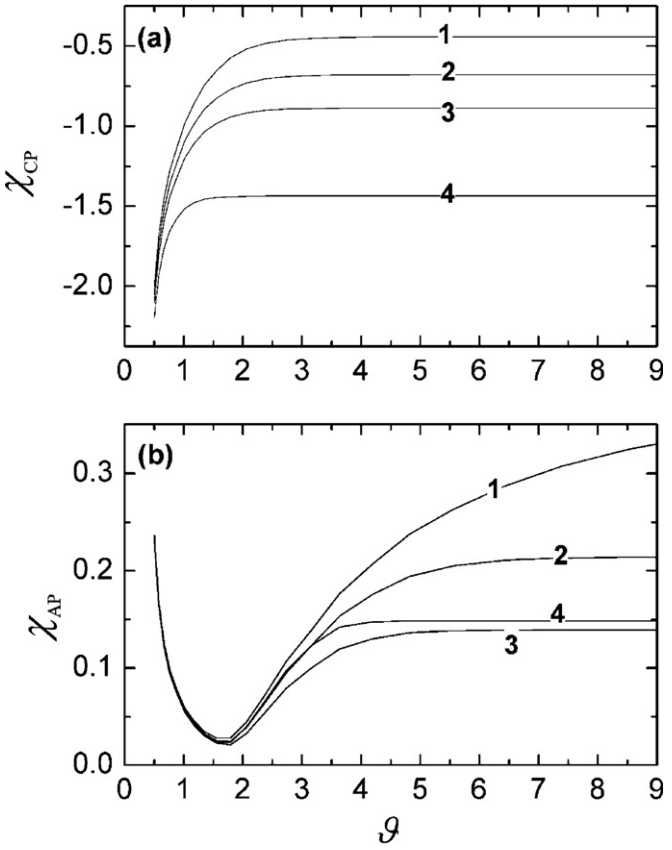


**Fig. 6.** Dimensionless current peak as function of the dimensionless thickness of the film, corresponding to different dimensionless chemical kinetic constant ($k_{c,M}$) and initial redox film concentration ($f^0_Q$): (1) $k_{c,M} = 0.0$, $f^0_Q = 0.0$; (2) $k_{c,M} = 1.0 \times 10^{-4}$, $f^0_Q = 5.0$; (3) $k_{c,M} = 1.0 \times 10^{-4}$, $f^0_Q = 10.0$; (4) $k_{c,M} = 5.0 \times 10^{-4}$, $f^0_Q = 10.0$. (a) Reduction peak current, $\chi_{CP}$ and (b) oxidation peak current, $\chi_{AP}$. Other simulation parameters: $P_o = 30.0$, $P_f = -30.0$, $\zeta_1 = 1.0$, $-\log\zeta_2 = -\log\zeta_3 = 4.0$, $N_P = 1000$.

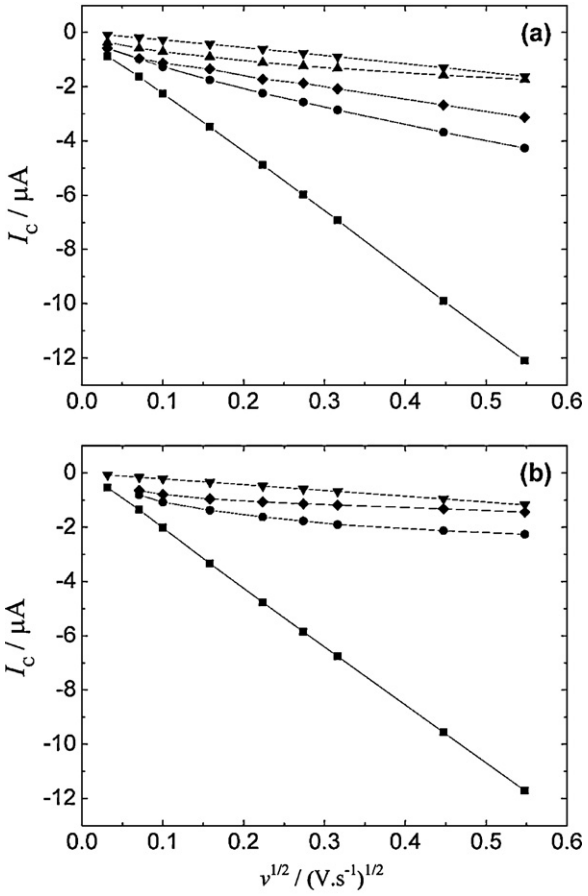


**Fig. 7.** Reduction peak current dependence of the square root of sweep potential rate for the transfer of 1 mM $Ru(NH_3)_6^{3+}$. (a) Experimental data: (▼) CHI|Au6, (♦) CHI|AU120, (▲) CHI|AU200, (●) CHI|AU250, (■) bare electrode; (b) numeric simulation at different film thicknesses: (▼) 500 μm, (♦) 1 μm, (●) 0.5 μm, (■) bare electrode. Simulation parameters: $D_O^b = D_R^b = 3.8 \times 10^{-10}$ m$^2$ s$^{-1}$; $D_O^{TF} = D_R^{TF} = 7.0 \times 10^{-12}$ m$^2$ s$^{-1}$; $A = 0.042$ cm$^2$; $f_Q^0 = 0.0$; $k_c = 0.0$ dm$^3$ mol$^{-1}$ s$^{-1}$; $N_P = 500{,}000$.

thickness ($\vartheta < 2$) but changes in the voltammetric profiles given by the coupled homogeneous reaction are more evident at high values of dimensionless thickness ($\vartheta < 2$). This latter fact allows for a discrimination of the experimental conditions that are useful to quantify diffusion related processes or the chemical kinetic of the coupled reaction. In order to have a clear idea of the required experimental conditions a typical case is exemplified. Let us consider the results shown in Fig. 6, a dimensionless thickness higher than 3 is enough to ensure a behavior controlled by the kinetic of the coupled chemical reaction. This value, $\vartheta = 3$, for a typical scan rate of 0.10 V s$^{-1}$ and diffusion coefficients in the order of $5 \times 10^{-6}$ cm$^2$ s$^{-1}$, correspond to a real thickness of ~30 μm, which is readily controlled by almost any film deposition technique. Of course, this rough analysis depends on the actual kinetic constant and different cases can be found.

### 4.3. Experimental validation

Experimental validation of the model is performed by simulation of the reduction of $Ru(NH_3)_6^{3+}$ on bare gold and film modified gold. In this last case, the electrode is modified with a film of cross-linked chitosan (CHI|Au6); or, alternatively, with a cross-linked chitosan film containing thionine (THI|CHI). Characterization of this system has been previously published [15].

Fig. 7(a) shows the peak current values plotted as a function of the square root of the sweep potential rate, for the reduction of

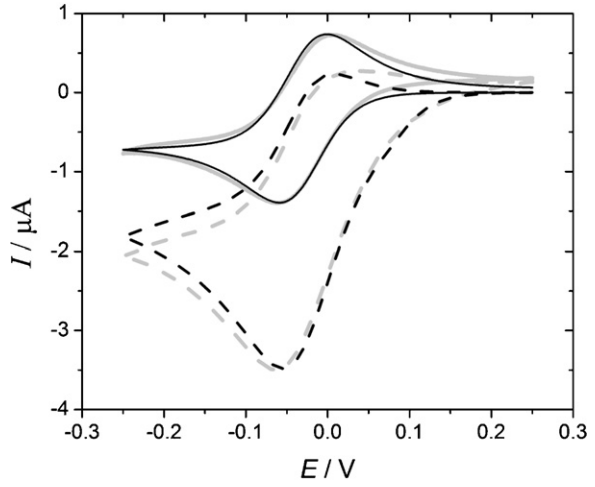


**Fig. 8.** Current–potential profiles corresponding to the heterogeneous transfer of 1.45 mM $Ru(NH_3)_6^{3+}$. Experimental data: (▬) CHI|Au6 and (▬) THI|CHI; simulated data: (╲) and (—) respectively. Experimental conditions: 5 mM $H_2SO_4$, $v = 0.100$ V s$^{-1}$, $A = 0.042$ cm$^2$. Simulation parameters: $v = 0.100$ V s$^{-1}$; film thickness = 5.7 μm; $D_O^b = D_R^b = 3.8 \times 10^{-10}$ m$^2$ s$^{-1}$; $D_O^{TF} = D_R^{TF} = 7.0 \times 10^{-12}$ m$^2$ s$^{-1}$; $A = 0.042$ cm$^2$; $f_Q^0 = 3.7$; $k_c = 1.0 \times 10^3$ m$^3$ mol$^{-1}$ s$^{-1}$; $N_P = 500{,}000$; $\delta t = 5.1 \times 10^{-7}$ s; $h^b = 2.1 \times 10^{-8}$ m; $h^{TF} = 2.8 \times 10^{-9}$ m. Reference electrode: Ag|AgCl|3M KCl.

$Ru(NH_3)_6^{3+}$, at the bare and electrodes modified with films of different thicknesses. The linear dependence found in bare and thick film electrodes (i.e. CHI|Au6) indicates that in these cases the heterogeneous charge transfer is reversible and controlled by diffusion of the electroactive species. Also it can be concluded from these results that the chitosan film is not forming a array of microholes on the surface of the electrode or at least the hole density is high enough to behave as a planar electrode. Linear fit of these dependences allows the determination of the diffusion coefficient of $Ru(NH_3)_6^{3+}$ in solution ($D_o^b = 3.8 \times 10^{-10}$m$^2$s$^{-1}$) and in the crosslinked chitosan film ($D_o^b = 7.0 \times 10^{-12}$m$^2$s$^{-1}$).

The same tendency is observed in the numerical simulations (Fig. 7b). When the thickness of the film is similar to the Nernst diffusion layer (i.e. intermediate thicknesses), the relationship departs from linearity. High potential sweep rates imply a Nernst layer thinner than the film, under this situation the diffusion is only defined by the lowest diffusion coefficient (i.e. diffusion coefficient inside the thin film). On the other side, smaller scan rates allow for the diffusion layer to extend beyond the film, were the diffusion of species in the solution begins to be important.

Both, simulation and experimental data show that the lower the film thickness, the greater the contribution of $D_o^b$, and the profile tends to resemble that diffusion profile for the reduction of $Ru(NH_3)_6^{3+}$ at the bare electrode.

When thionine is immobilized in the polymeric film it reacts irreversibly with the reduced $Ru(NH_3)_6^{2+}$ complex formed at the electrode. The changes produced in the voltammetric profile and the corresponding numerical simulation are shown in Fig. 8. An excellent correlation is evident from the comparison of simulated and experimental profiles in both cases that is, with and without thionine. A film thickness of 5.7 μm and a kinetic constant of $1.0 \times 10^6$ M$^{-1}$ s$^{-1}$ for the coupled homogeneous reaction were obtained.

## 5. Conclusions

Cyclic voltammograms corresponding to a catalytic EC′ reaction taking place at a thin film modified electrode were numerically simulated in the present paper. The model considers the difference in diffusion coefficients in the thin film layer and in the bulk

solution. In absence of redox immobilized species, that is, when only the electroactive compound is present, diffusion coefficient inside and outside the film, sweep rate, thickness of the film, determine not only the shape of the voltammogram but also the tendency in linearity of the peak current with the square root of sweep potential rate. For very thick films the electrochemical response is very similar to that observed on bare electrodes, but with a very low diffusion coefficient.

The electrochemical reduction of $Ru(NH_3)_6^{3+}$ on a gold electrode followed by the homogenous reaction with immobilized thionine in a chitosan film to regenerate the oxidized $Ru(NH_3)_6^{3+}$ complex, was chosen as experimental system to validate the model.

An important result of this paper is that in the presence of thionine in the experimental system, it is possible to obtain the kinetic constant for the catalytic homogeneous reaction when it takes place in thick films, as can clearly be observed in Fig. 6.

Summing up the working curves obtained with the model allowed us to quantify diffusion coefficients of the electroactive species in film and solution, the homogeneous kinetic constant of the reaction between this and the immobilized species, and the thickness of the thin layer in a real system under certain experimental conditions.

## Acknowledgements

The research described herein was funded by Consejo Nacional de Investigaciones Científicas y Técnicas (CONICET), Fondo Nacional de Ciencia y Tecnología (FONCYT) and Secretaria de Ciencia y Técnica (SECYT-UNC). L.G. also acknowledges the support of CONICET for providing the research fellowship.

## References

[1] Heller, B. Feldman, Electrochemical glucose sensors and their applications in diabetes management, Chemical Reviews 108 (2008) 2482.
[2] T. Ahuja, I.A. Mir, D. Kumar, Rajesh, Biomolecular immobilization on conducting polymers for biosensing applications, Biomaterials 28 (2007) 791.
[3] T.E. Benavidez, A.M. Baruzzi, Comparative behavior of glucose oxidase and oxalate oxidase immobilized in mucin/chitosan hydrogels for biosensors applications, Polymer 53 (2012) 438.
[4] F. Li, W. Chen, S. Zhang, Development of DNA electrochemical biosensor based on covalent immobilization of probe DNA by direct coupling of sol–gel and self-assembly technologies, Biosensors and Bioelectronics 24 (2008) 781.
[5] T.Q. Huy, N.T.H. Hanh, N.T. Thuy, P.V. Chung, P.T. Nga, M.A. Tuan, A novel biosensor based on serum antibody immobilization for rapid detection of viral antigens, Talanta 86 (2011) 271.
[6] M. García-Heras, C. Gil, N. Carmona, J. Faber, K. Kromka, M.A. Villegas, Optical behavior of pH detectors based on sol–gel technology, Analytica Chimica Acta 540 (2005) 147.
[7] G. Beltran-Pérez, F. Lopez-Huerta, S. Munoz-Aguirre, J. Castillo-Mixcoatl, R. Palomino-Merino, R. Lozada-Morales, O. Portillo-Moreno, Fabrication and characterization of an optical fiber pH sensor using sol–gel deposited $TiO_2$ film doped with organic dyes, Sensors and Actuators B 120 (2006) 74.
[8] M.-S. Chiou, P.-Y. Ho, H.-Y. Li, Adsorption of anionic dyes in acid solutions using chemically cross-linked chitosan beads, Dyes and Pigments 60 (2004) 699.
[9] J. Goicoechea, C.R. Zamarreno, I.R. Matías, F.J. Arregui, Optical fiber pH sensors based on layer-by-layer electrostatic self-assembled neutral red, Sensors and Actuators B 132 (2008) 305.
[10] N. Raoufi, F. Surre, T. Sun, M. Rajarajan, K.T.V. Grattan, Wavelength dependent pH optical sensor using the layer-by-layer technique, Sensors and Actuators B 169 (2012) 374.
[11] K. Thenmozhi, S.S. Narayanan, Electrochemical sensor for $H_2O_2$ based on thionin immobilized 3-aminopropyltrimethoxy silane derived sol–gel thin film electrode, Sensors and Actuators B 125 (2007) 195.
[12] P. Hashemi, M. Hosseini, K. Zargoosh, K. Alizadeh, High sensitive optode for selective determination of $Ni^{2+}$ based on the covalently immobilized thionine in agarose membrane, Sensors and Actuators B 153 (2011) 24.
[13] Q.-J. Ma, H.-P. Li, F. Yang, J. Zhang, X.-F. Wu, Y. Bai, X.-F. Li, A fluorescent sensor for low pH values based on a covalently immobilized rhodamine–napthalimide conjugate, Sensors and Actuators B 166–167 (2012) 68.
[14] T.E. Benavidez, C.I. Alvarez, A.M. Baruzzi, Physicochemical properties of a mucin/chitosan matrix used for the development of an oxalate biosensor, Sensors and Actuators B 143 (2010) 660.
[15] L. Gerbino, J. Riva, M. Strumia, R.A. Iglesias, A.M. Baruzzi, Thionine immobilized in crosslinked chitosan films, Sensors and Actuators B: Chemical 131 (2008) 455.
[16] D. Britz, Digital Simulation in Electrochemistry (Lecture Notes Physics), 666, Springer, Heidelberg, Berlin, 2005.
[17] D.K. Gosser, Cyclic Voltammetry: Simulation and Analysis of Reaction Mechanisms, Wiley-VCH, New York, NY, USA, 1993.
[18] S.W. Feldberg, in: A.J. Bard (Ed.), Electroanalytical Chemistry, vol. 3, Marcel Dekker, New York, 1969, p. 271.
[19] L.K. Bieniasz, The von Neumann stability of finite-difference algorithms for the electrochemical kinetic simulation of diffusion coupled with homogeneous reactions, Journal of Electroanalytical Chemistry 345 (1993) 13.